Pergamon

Acta mater. Vol. 46, No. 8, pp. 2573–2585, 1998

Printed in Great Britain
PII: S1359-6454(97)00478-3
1359-6454/98 $19.00 + 0.00

COMPUTER SIMULATION OF STRESS-ORIENTED NUCLEATION AND GROWTH OF θ' PRECIPITATES IN Al–Cu ALLOYS

D. Y. LI† and L. Q. CHEN

Department of Materials Science and Engineering, The Pennsylvania State University, University Park, PA 16802, U.S.A.

(Received 10 September 1997; accepted 25 November 1997)

Abstract—Many structural transformations result in several orientation variants whose volume fractions and distributions can be controlled by applied stresses during nucleation, growth or coarsening. Depending on the type of stress and the coupling between the applied stress and the lattice misfit strain, the precipitate variants may be aligned parallel or perpendicular to the stress axis. This paper reports our studies on the effect of applied stresses on nucleation and growth of coherent θ' precipitates in Al–Cu alloys using computer simulations based on a diffuse-interface phase-field kinetic model. In this model, the orientational differences among precipitate variants are distinguished by non-conserved structural field variables, whereas the compositional difference between the precipitate and matrix is described by a conserved field variable. The temporal evolution of the spatially dependent field variables is determined by numerically solving the time-dependent Ginzburg–Landau (TDGL) equations for the structural variables and the Cahn–Hilliard diffusion equation for composition. Random noises were introduced in both the composition and the structural order parameter fields to simulate the nucleation of θ' precipitates. It is demonstrated that although an applied stress affects the microstructural development of a two-phase alloy during both the nucleation and growth stages, it is most effective to apply stresses during the initial nucleation stage for producing anisotropic precipitate alignment. © *1998 Acta Metallurgica Inc.*

1. INTRODUCTION

Stressed aging is one of efficient treatments for controlling the spatial arrangement of coherent precipitate variants [1–5]. A coherent phase transformation with a point symmetry reduction usually produces a number of variants which are oriented in different but equivalent crystallographic directions [1, 6]. An anisotropic distribution of the variants could be introduced by applying stress during aging [1, 2, 7, 8], and this anisotropic distribution may result in anisotropic behavior of a two-phase material. For instance, the tetragonal coherent θ' precipitate in an Al–Cu alloy has six variants with their plane respectively parallel to {100} planes of the matrix. If an initial homogeneous Al–Cu alloy is aged within the two-phase region of θ' and Al matrix without any external constraint, all the differently oriented variants will grow with the same probability. However, when the θ' precipitation proceeds under an applied stress, only some of θ' variants may develop preferentially, leading to an anisotropic distribution of θ' variants such as a parallel alignment of the θ' variants. The stress-orienting effect on θ' precipitation was studied by a number of researchers [3–5]. Eto *et al.* [4] observed that a tensile stress may align θ' precipitates along the axis of the stress, whereas a compressive stress makes the θ' precipitates perpendicular to the axis of the compressive stress. The stress-orienting effect on θ' precipitation was also observed by Skrotzki *et al.* [5] and Hosford *et al.* [3], respectively. However, it was not clear that the stress-orienting process occurs primarily during nucleation or during variant growth and coarsening. Sauthoff [9–11] found that the stress-orienting effect occurs mainly by selective coarsening, and the effect on nucleation is smaller. He discussed the effects of the orienting energy on nucleation, growth, and coarsening, and demonstrated that the precipitate orienting is feasible primarily by coarsening. However, Eto *et al.* [4] observed that in an Al–Cu alloy which was subject to an initial stress-free aging for a very short period followed by a stressed aging for a long period, all θ' variants appeared and there was little stress-orienting effect. On the other hand, by applying stress during aging for an initial short period followed by stress-free aging for a long period, they observed that θ' precipitates were aligned in parallel. It therefore seems that an applied stress has a strong effect on nucleation or initial precipitation process. Because of the experimental difficulty in studying nucleation, the question still remains open: does the stress-orienting effect occur primarily during nucleation or during growth and coarsening?

†Present address: Department of Chemical and Materials Engineering, University of Alberta, Edmonton, Alberta, Canada, T6G 2G6.

The main objective of the present study is, therefore, to distinguish the stress effect on the selective nucleation-and-growth and the selective variant coarsening by using computer simulation, with the aim of answering the question whether the stress-orienting effect primarily takes place during nucleation-and-growth or during variant coarsening. A diffuse-interface phase-field kinetic model based on the time-dependent Ginzburg–Landau and Cahn–Hilliard diffusion equations was employed [12–14, 38]. By introducing random noises in the composition and the structural order parameter fields, the nucleation of precipitates can be simulated. Therefore, the stress-orienting effects on both the selective nucleation and during growth and coarsening could be investigated. In particular, we consider the precipitation of θ' in Al–Cu alloys. The θ' precipitate is a coherent second phase which greatly enhances the strength of Al–Cu alloys. This precipitate phase has a tetragonal structure, and there is a large negative misfit (about −4.5%) between the θ' phase and the Al matrix along $\langle 001\rangle_{\theta'} \| \langle 001\rangle_{\mathrm{Al}}$ direction [15, 16]. The lattice mismatch is of particular importance to determining both the morphology of a coherent variant and the spatial arrangement of differently oriented variants [7, 8, 17–20].

2. DESCRIPTION OF THE DIFFUSE-INTERFACE FIELD MODEL

2.1. Representation of a two-phase microstructure

In the diffuse-interface field model, a microstructure is described by a set of spatially dependent field variables. The precipitate phase (θ') and the matrix (Al) under study differ not only in composition but also in structure. These differences are distinguished respectively by using a composition field variable, $C(\boldsymbol{r}, t)$, and long-range structural order parameters, $\eta_i(\boldsymbol{r}, t)$, where the subscript, i, corresponds to differently oriented variants of the precipitate phase. The former distinguish the compositional difference between the precipitate and the matrix, while the latter distinguish the structural difference between the precipitate and the matrix and also distinguish differently oriented variants of the precipitate phase. These field variables are continuous across the interphase boundaries. The microstructure of a multi-variant two-phase mixture can be represented by plotting either the composition field, $C(\boldsymbol{r}, t)$, or the structural order parameter variables, $\Sigma_i \eta_i^2(\vec{r}, t)$. Figure 1 schematically illustrates a multi-variant microstructure represented by the field variables.

2.2. The driving force for microstructural evolution

According to thermodynamic laws, the equilibrium state of a multi-phase system corresponds to the minimum free energy. The system is driven towards its equilibrium state by the reduction in free energy. The driving force for the temporal evolution of a coherent multiphase microstructure consists of the following contributions: (1) the reduction in the chemical free energy; (2) the decrease in the total interfacial energy of interphase boundary between different phases and boundaries or between differently oriented variants; (3) the relaxation of the elastic strain energy caused by the lattice mismatch between the matrix and the precipitate phase; and (4) the reduction in the coupling potential energy between the internal strain and external load, i.e., a constant applied strain or stress. In the present model, all these contributions

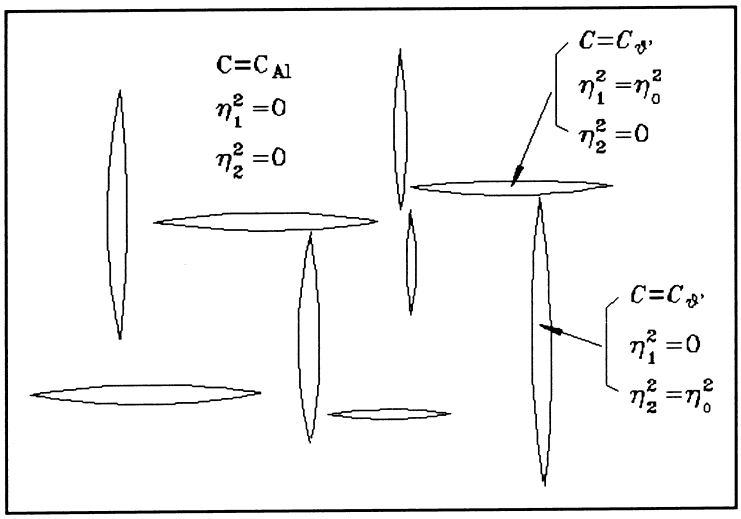

Fig. 1. A schematic illustration of a multi-variant two-phase mixture represented using the fields of composition and structural order parameters. There are two pairs of conjugate variants which are oriented in four directions and represented by ($\eta_1 = \pm\eta_o$, $\eta_2 = 0$) and ($\eta_1 = 0$, $\eta_2 = \pm\eta_o$), respectively. There is a 180° difference in orientation between each pair of the conjugate variants.

to the total free energy are included and expressed in terms of the field variables, $C(\boldsymbol{r}, t)$ and $\eta_p(\boldsymbol{r}, t)$.

2.2.1. The chemical free energy. The growth of θ' precipitates is driven by the difference in chemical free energy between a supersaturated matrix and the equilibrium matrix containing the θ' precipitates. This difference in chemical free energy approximately determines the volume fraction of θ' phase. In the diffuse-interface field model, the local chemical free energy density is approximated using a Landau-type of free energy polynomial

$$f(C, \eta_p) = \frac{A_1}{2}(C - C_1)^2 + \frac{A_2}{2}(C - C_2)\sum_p^v \eta_p^2 - \frac{A_3}{4}\sum_p^v \eta_p^4 + \frac{A_4}{6}\sum_p^v \eta_p^6 + A_5\sum_{q\neq p}^v \eta_p^2\eta_q^2 + A_6\sum_{p\neq q, p\neq r}^v \eta_p^4(\eta_q^2 + \eta_r^2) + A_7\sum_{p\neq q\neq r}^v \eta_p^2\eta_q^2\eta_r^2 \quad (1)$$

where v is the number of orientation variants and p is the notation for pth variant. At a given composition, the local free energy function has a number of degenerate minima corresponding to the free energy of each orientation variant, respectively. Therefore, the free energy density as a function of composition for the precipitate phase can be obtained by minimizing f with respect to the structural order field variables at different compositions, i.e. $f(C, \eta_{po}(C))$. For the present case of θ' precipitation in an Al–Cu alloy, the coefficients in equation (1) were chosen as follows: $A_1 = 54.0$, $A_2 = -17.0$, $A_3 = 7.0$, $A_4 = 2.5$, and $A_5 = A_6 = A_7 = 0.2$. (The free energy was measured in a unit, $mk_BT \approx 10^8$ ergs/cm^3, where $T = 443^\circ$K, m is a normalization coefficient equal to 1.63×10^{21} cm^{-3}.) C_1 and C_2 are constants respectively close to compositions of the aluminum matrix and the θ' phase, and their values are chosen as $C_1 = 0$ and $C_2 = 0.44$. Figure 2 illustrates the chemical free energies as a function of C: one curve corresponds to the matrix (Al) and the other corresponds to the θ' phase. This chemical free energy function provides equilibrium compositions of the precipitate phase and the matrix in the stress-free state as well as the chemical driving force for precipitation.

2.2.2. The interfacial energy. In a compositionally and/or structurally inhomogeneous solid, the interphase boundary energy also contributes to the system's total free energy. In the present simulation study, we assume that the interfacial energy is crystallographically isotropic, and it may be accounted by evaluating the energy contribution from the gradient terms in C and η_p fields. The total chemical free energy of an inhomogeneous system may thus be expressed as [12–14]

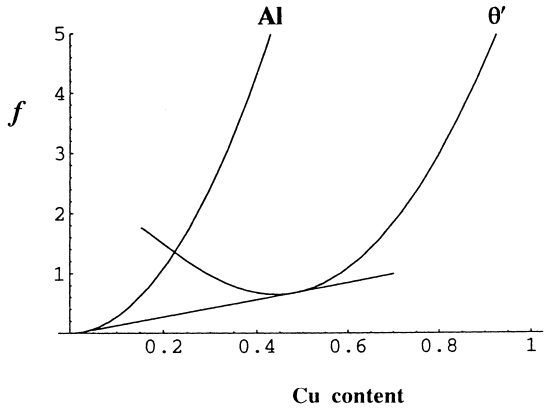

Fig. 2. Chemical free energies of θ' phase and the matrix of Al–Cu alloy vs composition.

$$F_c = \int_V [f(C, \eta_p(\boldsymbol{r})) + \sum_{p=1}^v \frac{\alpha_p}{2}(\nabla\eta_p(\boldsymbol{r}))^2 + \frac{\beta}{2}(\nabla C(\boldsymbol{r}))^2]\, d^3\boldsymbol{r} \quad (2)$$

where α_p and β are gradient energy coefficients. The integration is performed over the entire system. The total interfacial energy of the system is defined as the excess free energy associated with the interfaces, i.e.,

$$\sigma_{tot} = \iint\Big[f(C, \eta_p) - f_o(C) + \sum_{p=1}^v \frac{\alpha_p}{2}(\nabla\eta_p)^2 + \frac{\beta}{2}(\nabla C)^2\Big]\, d^3\boldsymbol{r} \quad (3)$$

where

$$f_o(C) = f(C_{\theta'}, \eta_{po}(C_{\theta'})) + \frac{f(C_{\theta'}, \eta_{po}(C_{\theta'})) - f(C_m, \eta_p = 0)}{C_{\theta'} - C_m}(C_o - C_{\theta'}) \quad (4)$$

where $C_{\theta'}$ and C_m are compositions of the precipitate and the matrix, respectively. C_o is the average composition of the system.

2.2.3. Elastic strain energy. An important contribution to the total free energy of a coherent two-phase mixture system comes from the elastic energy which is caused by the lattice mismatch between the precipitate and the matrix. Since the lattice mismatch is crystallographically anisotropic, the resultant coherent strain is anisotropic and this plays the major role in determining the morphological evolution (shape and orientation) of a precipitate variant. In addition, the long-range elastic interactions between different variants affect the growth of each single variant and thus strongly influence the mutual spatial arrangement of differently oriented variants of the precipitate phase.

Eshelby developed an elastic theory in 1957 for calculating the elastic strain of an ellipsoidal inclusion in an isotropic matrix based on the assumption that both phases have the same elastic moduli [21, 22]. By changing the ratios in length between different axes of the ellipsoidal inclusion, one may use Eshelby's theory to estimate the elastic energy of a coherent inclusion which may have different shapes such as a sphere, a disk, or a needle. Eshelby's theory has been later on modified and developed by many researchers [23–28]. Walpole [23], Kinoshita and Mura [24], and Asaro and Barnett [25] subsequently proved or extended Eshebly's theory to the anisotropic elastic cases. Lee *et al*. [27] numerically calculated the anisotropic elastic strain energy of coherent ellipsoidal precipitates and compared the results with those obtained using the isotropic elasticity theory. An alternative elastic theory of coherent two-phase systems in the homogeneous modulus approximation was proposed by Khachaturyan [17, 29, 30]. This theory is general and can be used to calculate a coherent inclusion with an arbitrary morphology. Khachaturyan theory has been extended to elastically inhomogeneous solids, i.e. the solids which contain phases having different elastic moduli [31]. This elastic theory was recently applied to the microstructural evolution in coherent multiphase materials [7].

In an Al–Cu alloy, the precipitate phase, θ', has a tetragonal crystal structure with $a_{\theta'} = 4.04$ Å and $c_{\theta'} = 5.80$ Å. While the matrix has a f.c.c. structure with $a_{\mathrm{Al}} = 4.049$ Å. This structural difference between θ' phase and the matrix causes a misfit strain. Since the difference between the lattice parameters along the c-direction is so large, the interfaces parallel to the c-direction can not be fully coherent. Dahmen and Westmacott [15] suggested that the θ' phase has a vacancy-type misfit of -4.5% in $(001)_{\theta'}||(001)_{\mathrm{Al}}$ when a two-unit cell θ' precipitate is fitted into three unit cells of the Al-matrix. Their suggestion is consistent with experiment studies conducted by Stobbs and Purdy [16]. Therefore, $\varepsilon^0_{(001)} = -0.045$ is used for the present simulation study. The eigen-strain tensor matrix is thus represented as

$$\begin{pmatrix} -0.0022 & 0 & 0 \\ 0 & -0.0022 & 0 \\ 0 & 0 & -0.045 \end{pmatrix}. \tag{5}$$

In Khachaturyan theory, different phase domains in a two-phase microstructure are separated by sharp-interfaces. The spatial dependence of stress-free strain can be characterized by a so-called shape-function which is 1 within a precipitate and 0 in the matrix. In the diffuse-interface description, however, the stress-free strain should be expressed in terms of field variables since a interphase boundary has a certain thickness across which the field variables change gradually. We assume that the local stress-free transformation strain, $\varepsilon_{ij}^0(\boldsymbol{r})$, is primarily dependent on the structural order parameter

$$\varepsilon_{ij}^0(\boldsymbol{r}) = \sum_p^v \varepsilon_{ij}^0(p)\eta_p^2(\boldsymbol{r}) \tag{6}$$

where $\eta_p(\boldsymbol{r})$ is the normalized structural order parameter describing the pth variant, and $\varepsilon_{ij}^0(p)$ is the corresponding stress-free strain for the pth variant when $\eta_p(\boldsymbol{r}) = 1$. The elastic energy of a two-phase mixture can be calculated as a function of the eigen-strain and the order parameter fields [14, 32, 33]. The final expression of the elastic energy has the following form [8]

$$\begin{aligned} E_{\mathrm{el}} = {} & \frac{V}{2}\lambda_{ijkl}\bar{\varepsilon}_{ij}\bar{\varepsilon}_{kl} - V\lambda_{ijkl}\bar{\varepsilon}_{ij}\sum_p^v \varepsilon_{kl}^0(p)\overline{\eta_p^2(\boldsymbol{r})} \\ & + \frac{V}{2}\lambda_{ijkl}\sum_p^v\sum_q^v \varepsilon_{ij}^0(p)\varepsilon_{kl}^0(q)\overline{\eta_p^2(\boldsymbol{r})\eta_q^2(\boldsymbol{r})} \\ & - \frac{1}{2}\sum_p^v\sum_q^v \int \frac{\mathrm{d}^3\boldsymbol{g}}{(2\pi)^3} B_{pq}(\boldsymbol{n})\{\eta_p^2(\boldsymbol{r})\}_{\boldsymbol{g}}^*\{\eta_q^2(\boldsymbol{r})\}_{\boldsymbol{g}} \end{aligned} \tag{7}$$

where λ_{ijkl} is the elastic constant. $B_{pq}(\boldsymbol{n}) = n_i\sigma_{ij}(p)\Omega_{jk}(\boldsymbol{n})\sigma_{kl}(q)n_l$ and $\Omega_{jk}(\boldsymbol{n})$ is the reverse matrix of $\Omega_{jk}^{-1}(\boldsymbol{n}) = n_i\lambda_{ijkl}n_l$. $\boldsymbol{g}$ and $\boldsymbol{n} = \boldsymbol{g}/g$ are a vector and its corresponding unit vector in the reciprocal space, respectively. $\{\eta_q^2(\boldsymbol{r})\}_{\boldsymbol{g}}$ is the Fourier transform of $\eta_q^2(\boldsymbol{r})$ and $\{\eta_p^2(\boldsymbol{r})\}_{\boldsymbol{g}}^*$ is the complex conjugate of $\{\eta_p^2(\boldsymbol{r})\}_{\boldsymbol{g}}$. $\bar{\varepsilon}_{ij} = \bar{\varepsilon}_{ij}^0 + \bar{\varepsilon}_{ij}^{\mathrm{a}}$ is the homogeneous strain which contains the homogeneous strain, $\bar{\varepsilon}_{ij}^0$, caused by the presence of the precipitates and the applied strain, $\bar{\varepsilon}_{ij}^{\mathrm{a}}$. In equation (7), the fourth term represents the configuration energy which determines the morphological pattern of a multi-variant microstructure. The first and third terms are constants which are dependent on the eigen-strain and the applied load. These two terms do not affect the morphology of the two-phase system. The second term represents the elastic coupling between the applied stress or strain and the local strain. Since the eigen-strain matrixes of differently oriented variants have different values, the second term is therefore crystallographically anisotropic and this determines the growth behavior of each orientation variant under an applied stress or strain, thus leading to the selective growth of differently oriented variants. The details of the derivation of the elastic strain energy in the field model was given in another paper [8].

When a precipitation process is constrained by applying a constant strain or stress, the internal strain field in the two-phase system is changed by the applied strain or stress, resulting in a variation of the strain energy barrier to growth of the precipitate. There are two types of constraints [2, 8]. One

is the *strain-constraint*, in which the system is under a constant applied strain with the system's boundary fixed. The governing potential of the system is the Helmholtz free energy. The second type of constraint, called *stress-constraint*, is to apply a constant stress on the system without fixing the system's boundary. Under this condition, the system is subjected to a constant external force. In this case, the governing potential is the Gibbs free energy.

The strain-constraint and the stress-constraint are two constraint modes frequently used for stressed aging treatment. For the strain-constraint condition, since the boundary of the system is fixed, the total elastic energy is obtained by simply replacing the homogeneous strain in equation (7) by the applied homogeneous strain, i.e., $\bar{\varepsilon}_{ij} = \bar{\varepsilon}^{\mathrm{a}}_{ij}$,

$$E_{\mathrm{el}} = \frac{V}{2}\lambda_{ijkl}\bar{\varepsilon}^{\mathrm{a}}_{ij}\bar{\varepsilon}^{\mathrm{a}}_{kl} - V\lambda_{ijkl}\bar{\varepsilon}^{\mathrm{a}}_{ij}\sum_{p}^{v}\varepsilon^{0}_{kl}(p)\overline{\eta^{2}_{p}(\boldsymbol{r})} + \frac{V}{2}\lambda_{ijkl}\sum_{p}^{v}\sum_{q}^{v}\varepsilon^{0}_{ij}(p)\varepsilon^{0}_{kl}(q)\overline{\eta^{2}_{p}(\boldsymbol{r})\eta^{2}_{q}(\boldsymbol{r})} - \frac{1}{2}\sum_{p}^{v}\sum_{q}^{v}\int\frac{\mathrm{d}^{3}\boldsymbol{g}}{(2\pi)^{3}}B_{pq}(\boldsymbol{n})\{\eta^{2}_{p}(\boldsymbol{r})\}_{\boldsymbol{g}}{}^{*}\{\eta^{2}_{q}(\boldsymbol{r})\}_{\boldsymbol{g}} \quad (8)$$

where the second term represents the coupling between the transformation strain, $\varepsilon_{ij}{}^{0}(p)$, and the applied strain, $\bar{\varepsilon}^{\mathrm{a}}_{ij}$. For the present simulation, the microstructural evolution under the strain-constraint condition was studied. The treatment for the stress-constraint condition was given elsewhere [8]. Although the expression of elastic energy in the stress-constraint condition is slightly different from the strain-constraint condition, they may not cause a detectable difference in microstructures developed respectively under these two constraint conditions.

2.3. The evolution equations for microstructural evolution

In this field model, the temporal evolution of a microstructure is determined by solving the time-dependent Ginzburg–Landau equations [34] for the non-conserved structural order parameter field variables and the Cahn–Hilliard diffusion equation [35] for the conserved concentration field variable:

$$\frac{\partial\eta_{p}(\boldsymbol{r},\,t)}{\partial t} = -L_{p}\frac{\delta F}{\delta\eta_{p}(\boldsymbol{r},\,t)} + \zeta_{p}(\boldsymbol{r},\,t),$$

$$\frac{\partial C(\boldsymbol{r},\,t)}{\partial t} = M\nabla^{2}\frac{\delta F}{\delta C(\boldsymbol{r},\,t)} + \xi(\boldsymbol{r},\,t) \quad (9)$$

where the subscript p represents different types of variants and $p = 1, 2, \ldots, v$. v is the number of the precipitate variants which oriented in different directions. M and L_p are kinetic coefficients which characterize the atomic diffusivity and interface boundary mobility. F is the total free energy of the system which includes the chemical free energy, the interfacial energy, and the elastic strain energy. For the present simulation study, F is a Helmholtz free energy because of the strain-constraint condition (fixed system boundary). If the system is under a stress-constraint condition (free system boundary), F should be a Gibbs free energy [2, 8].

$\zeta_p(\boldsymbol{r},\,t)$ and $\xi(\boldsymbol{r},\,t)$ are the Langevin noise terms which generate Gaussian-distributed random noises and satisfy the requirements of the fluctuation–dissipation theorem [36]

$$\langle\zeta_{p}(\boldsymbol{r},\,t)\zeta_{p}(\boldsymbol{r}',\,t')\rangle = 2k_{\mathrm{B}}TL_{p}\delta(\boldsymbol{r}-\boldsymbol{r}')\delta(t-t') \quad (10)$$

$$\langle\xi(\boldsymbol{r},\,t)\xi(\boldsymbol{r}',\,t')\rangle = -2k_{\mathrm{B}}TM\nabla^{2}\delta(\boldsymbol{r}-\boldsymbol{r}')\delta(t-t') \quad (11)$$

where k_{B} is the Boltzmann constant and T is the temperature. The noise terms are related to thermal variations (acoustic phonons) which have short relaxation times. The noises cause localized fluctuations in the composition and the structural order parameter fields.

The variational derivatives of the total free energy with respect to the compositional and structural field variables are, respectively,

$$\frac{\delta F}{\delta C(\boldsymbol{r})} = \frac{\delta F_{\mathrm{c}}}{\delta C(\boldsymbol{r})} + \frac{\delta E_{\mathrm{el}}}{\delta C(\boldsymbol{r})} = A_{1}[C(\boldsymbol{r}) - C_{1}] + \frac{A_{2}}{2}\sum_{p}^{v}\eta^{2}_{p}(\boldsymbol{r}) - \beta\nabla^{2}C(\boldsymbol{r}) \quad (12)$$

$$\frac{\delta F}{\delta\eta_{p}(\boldsymbol{r})} = \frac{\delta F_{\mathrm{c}}}{\delta\eta_{p}(\boldsymbol{r})} + \frac{\delta E_{\mathrm{el}}}{\delta\eta_{p}(\boldsymbol{r})} \quad (13)$$

where

$$\frac{\delta F_{\mathrm{c}}}{\delta\eta_{p}(\boldsymbol{r})} = \eta_{p}(\boldsymbol{r})\Bigg\{A_{2}(C - C_{2}) - A_{3}\eta^{2}_{p}(\boldsymbol{r}) + A_{4}\eta^{4}_{p}(\boldsymbol{r}) + 2A_{5}\sum_{q\neq p}^{v}\eta^{2}_{q}(\boldsymbol{r}) + 2A_{6}\Bigg[2\eta^{2}_{p}(\boldsymbol{r})\Bigg(\sum_{q\neq p}^{v}\eta^{2}_{q}(\boldsymbol{r})\Bigg) + \Bigg(\sum_{q\neq p}^{v}\eta^{4}_{q}(\boldsymbol{r})\Bigg)\Bigg] + 2A_{7}\sum_{q\neq r\neq p}^{v}\eta^{2}_{q}(\boldsymbol{r})\eta^{2}_{r}(\boldsymbol{r})\Bigg\} - \alpha_{p}\nabla^{2}\eta_{p}(\boldsymbol{r}) \quad (14)$$

$$\frac{\delta E_{\mathrm{el}}}{\delta\eta_{p}} = 2\eta_{p}(\boldsymbol{r})\Bigg[-C_{ijkl}\bar{\varepsilon}^{\mathrm{a}}_{ij}\varepsilon^{0}_{kl}(p) + \sum_{q}^{v}[C_{ijkl}\varepsilon^{0}_{ij}(p)\varepsilon^{0}_{kl}(q)\eta^{2}_{q}(\boldsymbol{r}) - \{B_{pq}(\boldsymbol{n})\{\eta^{2}_{q}(\boldsymbol{r})\}_{\boldsymbol{g}}\}_{\boldsymbol{r}}]\Bigg] \quad (15)$$

where $\{B_{pq}(\boldsymbol{n})\{\eta_q{}^2(\boldsymbol{r})\}_{\boldsymbol{g}}\}_{\boldsymbol{r}}$ represents the inverse Fourier transform of $B_{pq}(\boldsymbol{n})\{\eta_q{}^2(\boldsymbol{r})\}_{\boldsymbol{g}}$.

2.4. Numerical solutions

Since the evolution parts of equation (9) are non-linear with respect to the field variables, they were solved numerically. We solved the kinetic equations in equation (9) using the semi-implicit Fourier–Spectral method [39]. In the Fourier space, the kinetic equations in equation (9) become

$$\frac{\partial \eta_p(\boldsymbol{g}, t)}{\partial t} = -L_p\left\{\frac{\delta F}{\delta \eta_p}\right\}_{\boldsymbol{g}} + \zeta_p(\boldsymbol{g}, t),$$

$$\frac{\partial C(\boldsymbol{g},t)}{\partial t} = -M\boldsymbol{g}^2\left\{\frac{\delta F}{\delta C}\right\}_{\boldsymbol{g}} + \xi(\boldsymbol{g},t) \qquad (16)$$

where $\{\ldots\}_{\boldsymbol{g}}$ is the Fourier transform of $(\ldots)$; $\eta_p(\boldsymbol{g}, t)$, $C(\boldsymbol{g}, t)$, $\xi(\boldsymbol{g}, t)$, and $\zeta_p(\boldsymbol{g}, t)$ are Fourier transforms of $\eta_p(\boldsymbol{r}, t)$, $C(\boldsymbol{r}, t)$, $\xi(\boldsymbol{r}, t)$, and $\zeta_p(\boldsymbol{r}, t)$, respectively. In the semi-implicit method, we treated the linear high-order terms implicitly and the non-linear terms explicitly, i.e.,

$$\frac{\eta_p^{n+1}(\boldsymbol{g}) - \eta_p^n(\boldsymbol{g})}{\Delta t} = -L_p\left[\left\{\frac{\partial f}{\partial \eta_p}\right\}_{\boldsymbol{g}}^n + \alpha_p g^2 \eta_p^{n+1}(\boldsymbol{g}) + \left\{\frac{\delta E_{\mathrm{el}}}{\delta \eta_p}\right\}_{\boldsymbol{g}}^n\right] + \zeta_p^n(\boldsymbol{g}),$$

$$\frac{C^{n+1}(\boldsymbol{g}) - C^n(\boldsymbol{g})}{\Delta t} = -Mg^2\left[\left\{\frac{\partial f}{\partial C}\right\}_{\boldsymbol{g}}^n + \beta g^2 C^{n+1}(\boldsymbol{g})\right] + \xi^n(\boldsymbol{g}). \qquad (17)$$

Starting with initial distributions of the non-conserved and conserved field variables, equation (17) can be solved iteratively to yield the time-dependence of the field variables, and thus the microstructural evolution.

3. RESULTS AND DISCUSSION

According to the change in symmetry, there are six possible orientation variants of the tetragonal θ' phase in a f.c.c. Al matrix, whose $[001]_{\theta'}$ axes are respectively parallel to six $\langle 100\rangle_{\mathrm{Al}}$ axes. x, y, z axes of the global coordinate frame are respectively parallel to $[100]_{\mathrm{Al}}$, $[010]_{\mathrm{Al}}$, $[001]_{\mathrm{Al}}$ of the matrix. In this coordinate, the eigen-strain matrixes of θ' phase variants are

$$\varepsilon^0_{ij_{[001]_{\theta'}\parallel[001]_{\mathrm{Al}}}} = \varepsilon^0_{ij_{[001]_{\theta'}\parallel[00\bar{1}]_{\mathrm{Al}}}} = \begin{pmatrix} -0.0022 & 0 & 0 \\ 0 & -0.0022 & 0 \\ 0 & 0 & -0.045 \end{pmatrix},$$

$$\varepsilon^0_{ij_{[001]_{\theta'}\parallel[010]_{\mathrm{Al}}}} = \varepsilon^0_{ij_{[001]_{\theta'}\parallel[0\bar{1}0]_{\mathrm{Al}}}} = \begin{pmatrix} -0.0022 & 0 & 0 \\ 0 & -0.045 & 0 \\ 0 & 0 & -0.0022 \end{pmatrix},$$

$$\varepsilon^0_{ij_{[001]_{\theta'}\parallel[100]_{\mathrm{Al}}}} = \varepsilon^0_{ij_{[001]_{\theta'}\parallel[\bar{1}00]_{\mathrm{Al}}}} = \begin{pmatrix} -0.045 & 0 & 0 \\ 0 & -0.0022 & 0 \\ 0 & 0 & -0.0022 \end{pmatrix}. \qquad (18)$$

The elastic constants of the Al matrix and the θ' precipitate phase were assumed to be the same, and elastic constants of aluminum were used for the simulation: $C_{11} = 1.08 \times 10^{12}$ ergs/cm^3, $C_{12} = 0.61 \times 10^{12}$ ergs/cm^3, and $C_{44} = 0.29 \times 10^{12}$ ergs/cm^3 [37].

The simulation was conducted in a two-dimensional space and four θ' variants were considered, which were distinguished by using two structural field variables, $\eta_1 = \pm\eta_{\mathrm{o}}$ and $\eta_2 = \pm\eta_{\mathrm{o}}$, respectively. A 256×256 uniform square grid was used to spatially discretize the field equations. The gradient coefficients α_p and β were assumed to be 1.5. The kinetic coefficients in equation (9) are assumed to be constant. L_p and M were chosen to be 0.4. In order to investigate the strain effect on the growth of θ' precipitates, compressive and tensile stresses, $\sigma = \mp 67$ MPa, were initially applied to the system to introduce compressive and tensile strain constraints (i.e., resulted in constraint strain ε^a), respectively. In the present simulation, the reduced time $t^* = t/t_{\mathrm{o}}$ was used to represent the "aging time", where $t_{\mathrm{o}} = (Lmk_{\mathrm{B}}T)^{-1}$. For each iteration, the time step is $\Delta t^* = 0.002$.

3.1. Morphology of a single θ' particle

The morphology of a coherent precipitate phase in a two-phase material affects the local strain state and is therefore of importance to properties of the material. In order to investigate morphological evolution of a single θ' particle in Al–Cu alloys, a spherical θ' particle (circle in 2D space) was embedded in a Al–Cu matrix with composition $C_{\mathrm{m}} = 0.06$. It was observed that a shape transformation took place as the "aging" proceeded. The particle changed its shape from a sphere to a thin disc with a thin cross section as shown in Fig. 3. This change in shape is attributable to the crystallographical anisotropy of the growth rate of the particle. Since the interfacial energy was assumed isotropic,

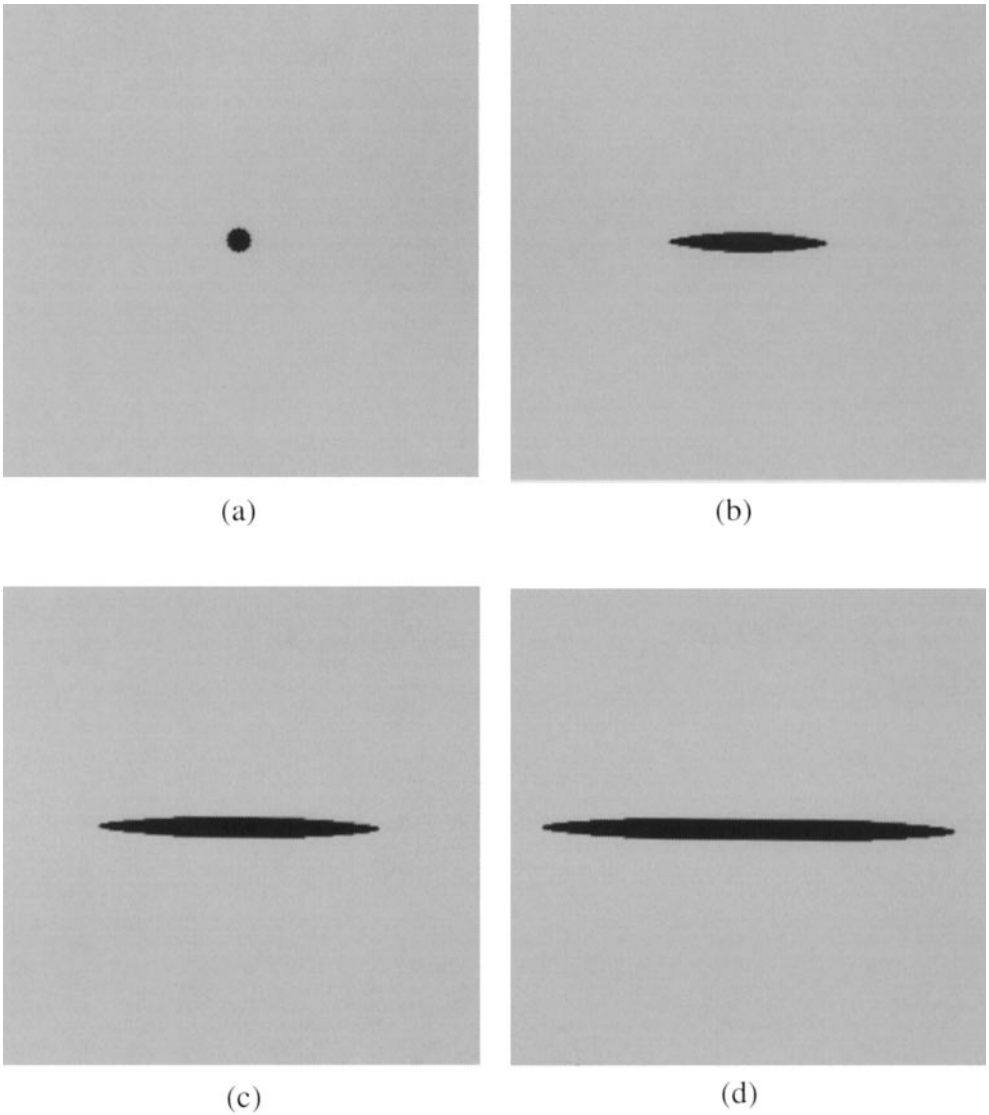

Fig. 3. A θ' particle changes from an initial sphere (square in 2D space) to a thin plate with a narrow leaf-like cross section under the influence of the coherent elastic energy. (a) $t^* = 0$, (b) $t^* = 900$, (c) $t^* = 1800$, (d) $t^* = 3000$.

this shape change is therefore mainly caused by the elastic energy which is a function of the shape and orientation of the particle. The morphology of a coherent precipitate is actually determined by the balance between the strain energy and the interphase boundary energy. However, the effect of interfacial energy is dominant only when the particle is small. As the particle grows bigger, the elastic energy becomes predominant, since the elastic energy increases faster (with r^3 where r is the dimension of the particle) than the interfacial energy (with r^2). Therefore, the particle has a critical size, larger than which the elastic energy has a predominant effect on the morphology of the particle. This critical size may be estimated in the following way [17]. The interfacial energy of a coherent precipitate is estimated as

$$E_s \sim S_p \cdot \gamma_s \tag{19}$$

where S_p is the surface area of the precipitate dependent on the precipitate shape, and γ_s is the interfacial energy dependent on the orientation of the precipitate. The coherent elastic energy may be estimated as

$$E_{el} \sim V_p \cdot \lambda \varepsilon_0^2 \tag{20}$$

where V_p is the precipitate volume, λ is the typical elastic modulus, and ε_0 is the typical stress-free transformation strain. The precipitate morphology is determined by minimizing

$$E_s + E_{el}.$$

We may estimate the ratio

$$\kappa = \frac{E_s}{E_{el}} \sim \frac{S_p \cdot \gamma_s}{V_p \cdot \lambda \varepsilon_0^2} \sim \frac{r_0}{(V_p/S_p)} \sim \frac{r_0}{r}. \qquad (21)$$

The critical size dimension is thus obtained by letting the ratio equal to the unity, that is

$$r_0 = \frac{\gamma_s}{\lambda \varepsilon_0^2}. \qquad (22)$$

When the size dimension of a particle is larger than r_0, i.e., $\kappa \sim r_0/r < 1$, the morphological evolution of the particle is dominated by the elastic strain energy; while the interfacial energy play a predominant role in the morphological evolution when the size dimension of the particle is smaller than r_o, i.e. $\kappa > 1$. For the particle illustrated in Fig. 3, its was calculated using equations (3) and (7), which respectively give values of the interfacial energy and the elastic energy. The obtained ratio is equal to $0.033 \ll 1$. The elastic energy is therefore predominant in determining the morphology of the θ' particle. The obtained interfacial energy has the value $\gamma_s = 179\ \mathrm{mJ/m^2}$, which is in the usual range of coherent interphase boundaries. Using this γ_s value, we estimated r_0 using equation (22) and obtained $r_0 \sim 0.8$ nm. Compared with experimentally observed θ' precipitates [4, 5] whose dimensions are usually in the region of 50 nm, it is obvious that their morphologies are dominated by the elastic energy.

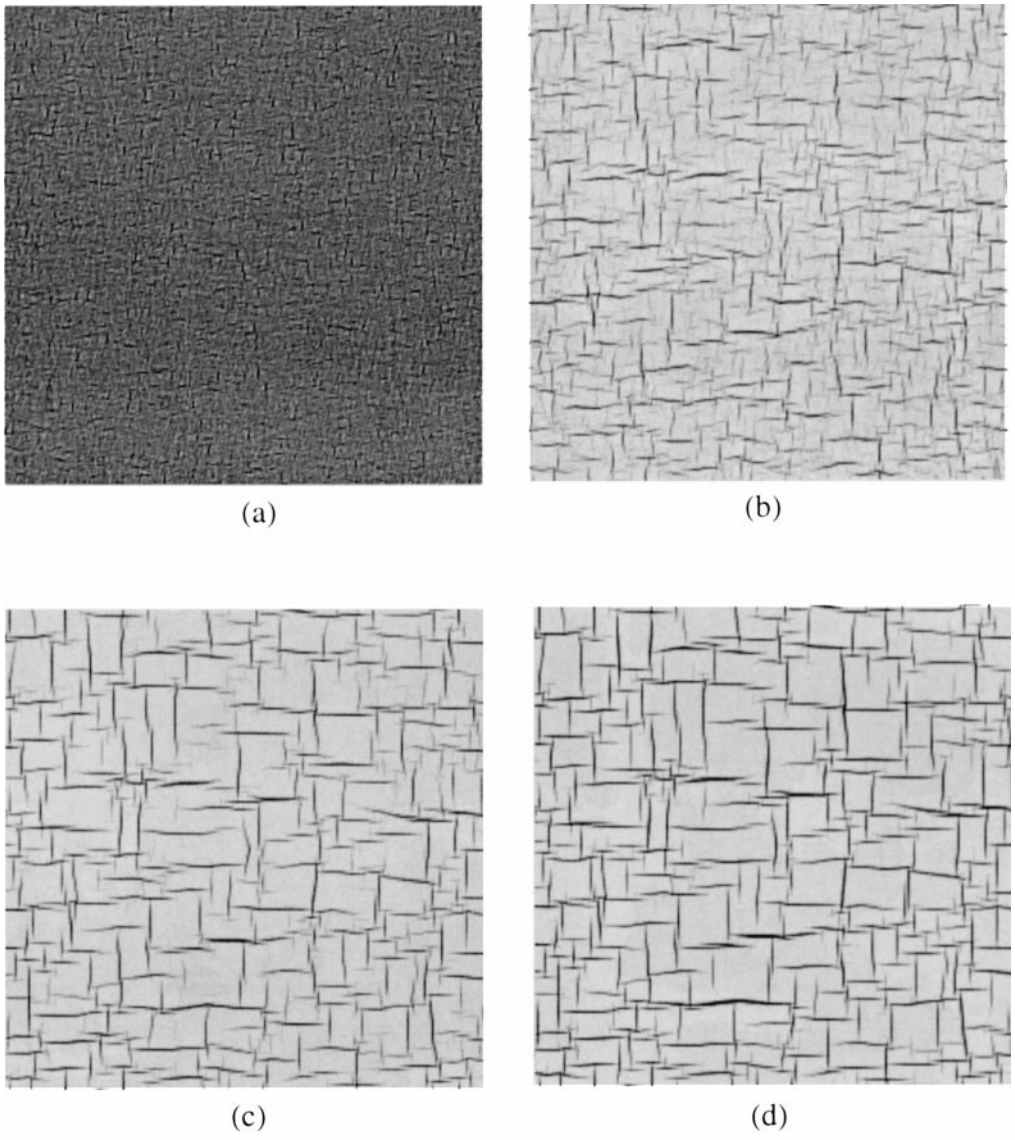

Fig. 4. Microstructural evolution in a Al–Cu alloy, starting from the nucleation caused by initial random fluctuations in the concentration field as well as in the structural order parameter fields. (a) $t^* = 70$, (b) $t^* = 700$, (c) $t^* = 3500$, (d) $t^* = 7000$.

3.2. Microstructural evolution and its variation with applied stresses

Microstructural evolution in a supersaturated Al–Cu alloy during nucleation and growth was simulated. The starting composition and structural order parameter fields were homogeneous, with $C_m(\vec{r}) = 0.06$ and $\eta_p(\vec{r}) = 0$. Nucleation was initiated by "turning on" the noise terms in equation (9) and was kept on for a certain period. The tetragonal θ' phase has three types of variants with their $(100)_{\theta'}$ (or $(\bar{1}00)_{\theta'}$) plane parallel to (100), (010) and (001) planes of the f.c.c. matrix, respectively. Since the simulation was carried out in a 2D space, only two types of θ' variants were considered. Each type of the variants include variants with a particular orientation and their conjugates, e.g., $(100)_{\theta'}||(100)$ variants and their conjugate, $(\bar{1}00)_{\theta'}||(100)$ variants. The simulated process of the microstructural evolution is illustrated in Fig. 4. The developed microstructure consists of two types of θ' variants which are perpendicular to each other. The simulated morphological pattern agrees very well with experimental observations [4, 5].

A tensile stress with the magnitude equal to 67 MPa was initially applied to a supersaturated Al–Cu system to establish a constant constraint strain. Under such a constraint strain, only one type of θ' variants grew preferentially along the stress orientation, thus forming a parallel alignment of the θ' variants as illustrated in Fig. 5(a). When the applied stress was changed to a compressive one, the favored θ' variants, however, became those perpendicular to the axis of the compressive stress (see Fig. 5(b)). The simulation agrees with the experiments conducted respectively by Eto *et al.* [4] and Skrotzki *et al.* [5], but contradicts that performed by Hosford and Agrawal [3]. On taking a close look at the eigen-strain of θ' phase (see equation (5)), one may see that the major component of the eigen-strain is a negative mismatch along z direction. This negative eigen-strain causes a tensile strain along the z direction. If a compressive external strain is applied along the z axis, it reduces this internal tensile strain and thus decreases the strain energy barrier to the growth of the precipitate, thus leading to preferential growth of the precipitate which lies perpendicular to the compressive stress. If a tensile stress is applied, however, it will increases this tensile strain and thus unfavors the growth of the precipitate. As a result, only those variants which lies along the tensile applied stress will grow selectively. It is not clear why a different stress-induced preferential alignment was observed by Hosford and Agrawal. This contradiction may be explained from possible variations in the lattice misfit. As suggested, small θ' precipitates have a negative misfit [15]. While the misfit may change its sign and magnitude during particle thickening [16]. It is noticed that the θ' precipitates observed by Hosford and Agrawal [3] are bigger than those observed by Eto *et al.* [4] and Skrotzki *et al.* [5]. If the eigen-strain changes its sign and becomes positive as the precipitate size increases, the preferential orientation of θ' precipitate under stresses may be along the directions observed by Hosford and Agrawal. However, whether or not this is true needs further studies.

3.3. The mechanism of the stress-orienting effect on the selective precipitation

An applied stress has a strong orienting effect on the formation of particularly oriented θ' precipitate variants. There are two possibilities for the for-

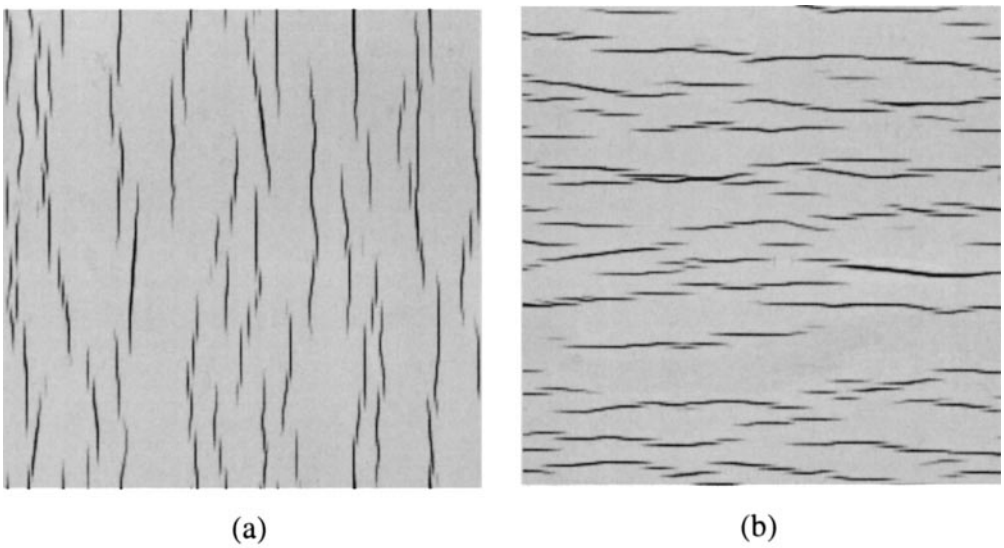

Fig. 5. Microstructures formed under external stresses applied vertically. (a) $\sigma = 67$ MPa, (b) $\sigma = -67$ MPa. $t^* = 7000$.

mation of parallel alignment of the selective θ' variants under the applied stress. One is the stress-selected nucleation and the other is the stress-selected variant growth. Which one is primarily responsible for the stress-orienting effect is still controversial. Sauthoff [9–11] found that the stress-orienting effect occurs mainly on the selective coarsening although there is also a smaller but observable effect on nucleation. Eto *et al.* [4] designed experiments to investigate the stress-orienting effect. In a stressed aging experiment, they applied a stress to a supersaturated specimen only at the beginning of the aging when the nucleation of θ' precipitates is predominant. Under such a condition, precipitated θ' variants were aligned in parallel. It thereby appears that the stress orienting effect is mainly on nucleation, i.e. under the applied stress only some particularly oriented nuclei can form, which result in the final parallel alignment of θ' variants with specific orientations. For a further confirmation, they also examined effects of a stress which was applied to a supersaturated specimen after initial five minutes of stress-free aging. The stressed aging lasted 32 hours. In this case, no parallel alignment of θ' variants was observed. Since during the initial five minutes of aging under stress-free condition various nuclei could form, the absence of parallel alignment of θ' variants indicates that a later applied stress did not cause a selective growth of initially formed θ' nuclei with different orientations. From the experiments, they suggested that the stress-orienting effect is a direct consequence of the formation of particularly oriented nuclei. However, the strain energy analysis in a Ni–Ti system made by Li and Chen [1] demonstrates that there is a strain energy barrier to the growth of a coherent precipitate due to the lattice mismatch. This energy barrier can be changed by the coupling between the coherent strain and the applied stress, which is crystallographically anisotropic. As a result, some variants of a coherent precipitate phase may grow preferentially and this leads to a parallel arrangement of the selectively grown variants. This coupling is always present from nucleation to coarsening. Therefore, the stress effect should exist during both the nucleation and growth. In order to justify this hypothesis and clarify the existing disagreement, the following simulation studies were performed.

Three simulation "experiments" were conducted. The entire "aging" was divided into two periods from $t^* = 0$ to $t^* = 1000$ and from $t^* = 1001$ to $t^* = 5000$. Nucleation was initiated by "turning on" the noise terms in equation (9) during the first period, while during the second period the noise terms were "turned off" so that only the growth of the precipitates was allowed. The initial composition and the structural order parameter fields were homogeneous, with $C_m = 0.06$ and $\eta_p = 0$. The following three conditions were tested.

(i) Constrained nucleation and stress-free growth.

In this case, the nucleation proceeded under a tensile stress applied vertically with its magnitude equal to 67 MPa, followed by a stress-free growth period. Figure 6(a) illustrates the microstructural evolution under such a constraint condition. It is clearly demonstrated that the constrained nucleation results in the formation of a group of particularly oriented precipitate variants. It thus appears that this preferentially oriented precipitation is attributed to the stress-orienting effect on the selective nucleation.

(ii) Stress-free nucleation and constrained growth.

In this case, no stress was applied during the nucleation period but the growth period proceeded under a tensile stress applied vertically with its magnitude equal to 67 MPa. Figure 6(b) illustrates the microstructural evolution under such a condition. Microstructural patterns taken at $t^* = 50$, $t^* = 500$, and $t^* = 5000$, respectively, are presented. In this case, no stress-orienting effect was observed. It seems that the stress-orienting effect is primarily on the selective nucleation rather than the selective variant growth. This is consistent with the conclusion drawn from the simulation performed under the condition (i).

(iii) Stress-free nucleation and constrained growth under a higher stress.

The simulation was performed under the condition similar to the condition (ii) but the constraint stress had a higher magnitude, $\sigma = 112$ MPa. The simulation demonstrates that under this higher stress the precipitate variants grew selectively and formed a parallel alignment as Fig. 6(c) illustrates. Since nuclei were generated without any applied constraints, this parallel alignment of particularly oriented variants is therefore attributed to the stress-induced selective variant growth.

From the above simulations, it is clear that the stress-orienting effect exists not only during nucleation but also during growth of coherent precipitate variants. The magnitude of the stress necessary to produce selective variant growth is, however, higher than that for the selective nucleation. This increase in the magnitude of the applied stress for selective variant growth is understandable from the viewpoint of the elastic interaction between θ' variants. In the stage of nucleation, the elastic interactions between different θ' nuclei are weak, because the elastic interaction energy of a pair of variants is dependent on their sizes and the inter-distance. As a result, each θ' nucleus may grow quite independently. When a stress is applied, whether or not a nucleus is elastically favored to grow is therefore dependent only on the coupling between its eigenstrain and the applied stress. Once the coupling results in a decrease in the elastic energy, a nucleus can continuously grow. However, this is not true during the variant growth stage. In a two-phase system with grown θ' precipitates, the elastic inter-

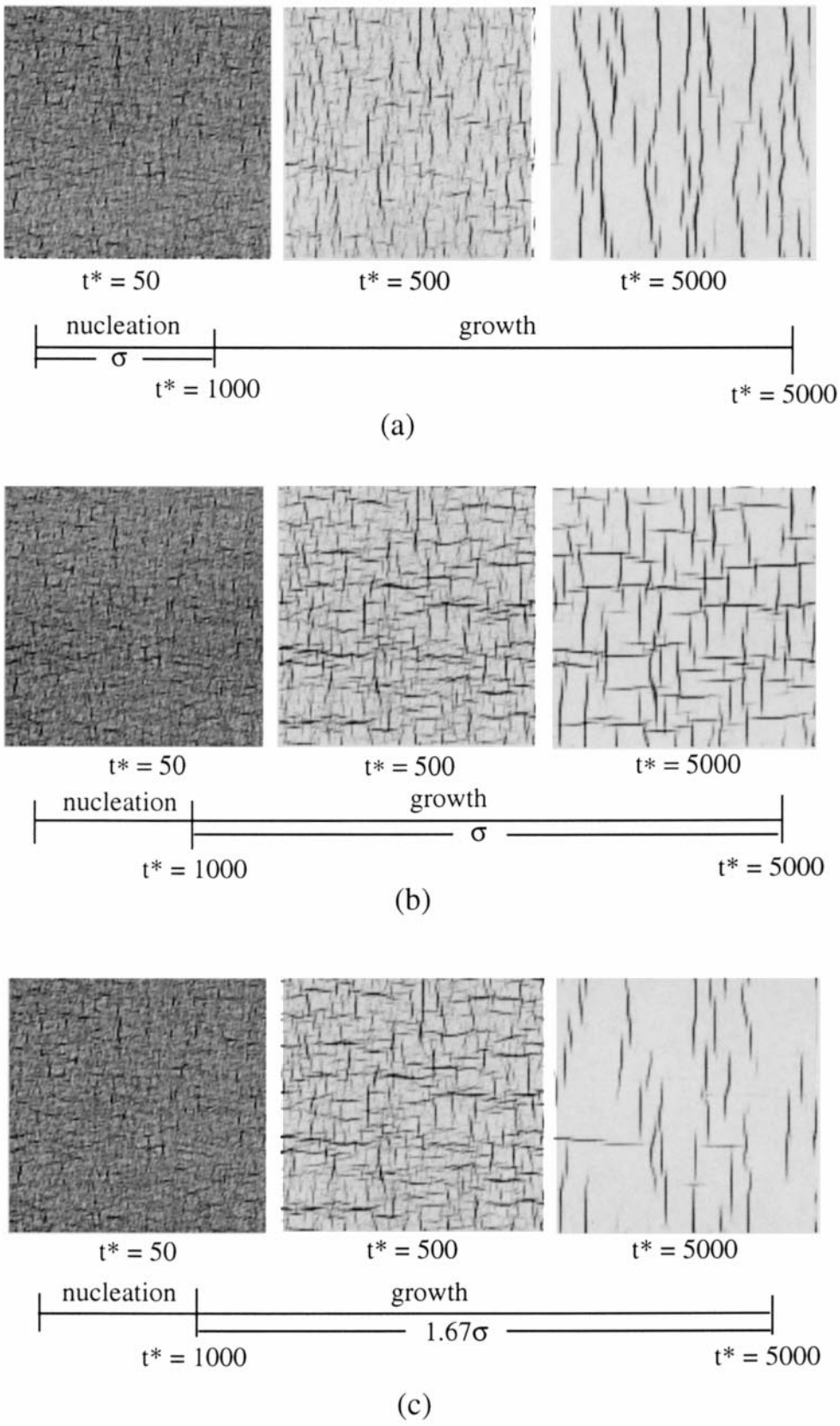

Fig. 6. Microstructural evolution under different constraint conditions: (a) constrained nucleation (σ = 67 MPa) followed by free variant growth, (b) free nucleation followed by constrained variant growth (σ = 67 MPa), and (c) free nucleation followed by constrained variant growth under a high stress (σ = 112 MPa).

action between the grown θ' variants is much stronger and this leads to a self-accommodative spatial distribution of the θ' variants to minimize the total elastic energy. To break this self-accommodative distribution and to produce a selective variant growth, an applied stress of higher magnitude is necessary to make the selective variant growth possible.

It should be pointed out, however, that the nucleation of θ' precipitates is a complicated process. It is generally believed that during this process GP zones are first formed, then a transition phase θ'' develops from the GP zones, followed by the formation of θ' precipitates which eventually transform to equilibrium θ phase. According to the classic interpretation [5, 40–43], θ' precipitates nucleate on either GP zones or θ'' precipitates. In the present study, nuclei of θ' precipitates were generated by introducing fluctuations in both the composition and the structural order parameter fields. The fluctuations do not necessarily provide embryos which have the same composition and order parameters as those the θ' precipitates have. In fact, some of these fluctuations gradually develop into θ' nuclei and the rest vanish under the influence of the thermodynamic driving force. This compositionally and structurally heterogeneous matrix may provide favorable sites for θ' nucleation as the GP zones and θ'' phase do. Although we did not simulate the particular process, GP *zones* $\rightarrow \theta'' \rightarrow \theta'$, it is expected that the applied stress has an effect on nucleation of GP zones and θ'' similar to that of θ'. Therefore, the fact that θ' phase may not directly nucleate from the matrix does not change our conclusion on the effect of applied stress on nucleation.

4. CONCLUSION

A computer simulation study was conducted to investigate microstructural evolution in an Al–Cu alloy containing coherent θ' precipitates, using a diffuse-interface field model. The stress-orienting effects on the selective nucleation and the selective variant growth of θ' precipitates were particularly studied. It was demonstrated that the growth of a θ' precipitate is strongly affected by internal and external strains. The high eigen-strain causing a large lattice mismatch makes the θ' precipitate a very thin disc. Under the influence of external stresses, the θ' precipitation becomes selective, resulting in parallel alignment of θ' precipitate variants. It is demonstrated that although the stress-orienting effect occurs during both nucleation and growth, it is more effective during the nucleation stage, in agreement with experimental observations.

Acknowledgements—This work is supported by both the Office of Naval Research Young Investigator Program under the grant number N-00014-95-1-0577 and the Pittsburgh Supercomputing Center. The simulation was performed in the Pittsburgh Supercomputing Center.

REFERENCES

1. Li, D. Y. and Chen, L. Q., *Acta mater*., 1997, **45**, 471.
2. Li, D. Y. and Chen, L. Q., *Acta mater*., 1997, **45**, 2435.
3. Hosford, W. F. and Agrawal, S. P., *Metall. Trans*., 1975, **6A**, 487.
4. Eto, T., Sato, A. and Mori, T., *Acta metall*., 1978, **36**, 499.
5. Skrotzki, B., Shiflet, G. J. and Starke, E. A. Jr., *Metall. Mater. Trans*., 1996, **27A**, 3431.
6. Portier, R. and Gratias, D., *J. de Phys. Colloque C* 4, supplement au No. 12, Tome 43, (1982) C4-17.
7. Li, D. Y. and Chen, L. Q., *Scripta mater*., 1997, **31,** 1271.
8. Li, D. Y. and Chen, L. Q., *Acta mater*., 1998, **46,** 639.
9. Sauthoff, G., *Z. Metallk*., 1977, **68**, 500.
10. Sauthoff, G., *Z. Metallk*., 1975, **66**, 106.
11. Sauthoff, G., *Z. Metallk*., 1976, **67**, 25.
12. Chen, L. Q. and Wang, Y., *J.O.M*., 1996, **48**, 13.
13. Wang, Y., Chen, L. Q. and Khachaturyan, A. G., in *Computer Simulation in Materials Science*, ed. H. O. Kirchner *et al.* Kluwer Academic Publishers, Netherlands, 1996, p. 325.
14. Fan, D. and Chen, L. Q., *J. Am. Ceram. Soc*., 1995, **78**, 769.
15. Dahmer, U. and Westmacott, K. H., *Physica status solidi (a)*, 1983, **80**, 249.
16. Stobbs, W. M. and Purdy, G. R., *Acta metall*., 1978, **26**, 1069.
17. Khachaturyan, A. G., *Theory of Structural Transformations in Solids*. John Wiley and Sons, New York, 1983.
18. Thompson, M. E., Su, C. S. and Voorhees, P. W., *Acta metall. mater*., 1994, **42**, 2107.
19. Khachaturyan, A. G., Semenovskaya, S. V. and Morris, J. W. Jr., *Acta metall*., 1988, **36**, 1563.
20. Lee, J. K., *Scripta metall. mater*., 1995, **32**, 559.
21. Eshelby, J. D., *Proc. R. Soc. A*, 1957, **241**, 376.
22. Eshelby, J. D., *Proc. R. Soc. A*, 1959, **252**, 561.
23. Walpole, L. J., *Proc. R. Soc. A*, 1967, **300**, 270.
24. Kinoshita, N. and Mura, T., *Physica status solidi (a)*, 1971, **5**, 759.
25. Asaro, R. J. and Barnett, D. M., *J. Mech. Phys. Solids*, 1975, **23**, 77.
26. Mura, T., Mori, T. and Kato, M., *J. Mech. Phys. Solids*, 1976, **24**, 305.
27. Lee, J. K., Barnett, D. M. and Aaronson, H. I., *Metall. Trans*., 1977, **8A**, 963.
28. Mori, T., Cheng, P. C., Kato, M. and Mura, T., *Acta metall*., 1978, **26**, 1435.
29. Khachaturyan, A. G., *Sov. Phys. Solid State*, 1967, **8**, 2163.
30. Khachaturyan, A. G. and Shatalov, G. A., *Sov. Phys. JETP*, 1969, **29**, 557.
31. Khachaturyan, A. G., Semenovskaya, S. and Tsakalakos, T., *Phys. Rev. B*, 1995, **52**, 1.
32. Chen, L. Q., Wang, Y. and Khachaturyan, A. G., *Phil. Mag. Lett*., 1992, **65**, 15.
33. Wang, Y., Wang, H., Chen, L. Q. and Khachaturyan, A. G., *J. Am. Ceram. Soc*., 1993, **76**, 3029.
34. Cahn, J. W. and Hilliard, J. E., *J. chem. Phys*., 1958, **28**, 258.
35. Allen, S. M. and Cahn, J. W., *Acta metall*., 1979, **27**, 1085.
36. Lifshitz, E. M. and Pitaevskii, L. P., *Landau and Lifshitz Course of Theoretical Physics*, Vol. 5. Pergamon Press, 1980.
37. Huntington, H. B., *The Elastic Constants of Crystals*. Academic Press, New York, 1958, p. 62.

38. Wang, Y., Chen, L. Q. and Khachaturyan, A. G., *Acta metall. mater*., 1993, **41**, 279.
39. Chen, L. Q. and Shen, J., to be published.
40. Porter, D. A. and Easterling, K. E., *Phase Transformations in Metals and Alloys*, 2nd ed. Chapman and Hall, London, 1992.
41. Berghezan, A., *The Mechanism of Phase Transformation in Metals*. Institute of Metals, London, 1956, p. 280.
42. Kelley, A. and Nicholson, R. B., *Prog. Mater. Sci*., 1963, **10**, 149.
43. Phillips, V. A., *Acta metall*., 1973, **21**, 219.